WILLIAM J. GECKLE and ROBIN RAUL

NUMERICAL AND EXPERIMENTAL SIMULATION OF CORONARY FLOW CHARACTERIZATION USING ARTERIOGRAPHY

Coronary arteriography is being used only for static imaging of vessel anatomy to assess coronary artery disease. We have completed a pilot study to establish the feasibility of extending this diagnostic technique to include images descriptive of the local flow in an artery. The study was undertaken to meet the need for flow-based measurements to clarify the relationship between blood flow and the frequent occurrence of postangioplasty complications. Our approach entails producing images that code fluid arrival times and turbulence as pixel intensities. This technique has been used successfully to reveal flow recirculation and turbulence zones in processed imagery from experimentally acquired arteriograms, and these results have been confirmed using numerical simulations. We have concluded that flow-sensitive imaging is possible from processed sequential arteriograms. Further development and testing of the method are therefore recommended to explore its usefulness as a diagnostic supplement to conventional coronary arteriography.

INTRODUCTION

Coronary angioplasty, which is discussed in greater detail in the next section, is a widely practiced procedure for relieving an artery of an atherosclerotic blockage. Unfortunately, for reasons that are not fully understood, 30% of the patients who undergo this treatment will experience restenosis (renarrowing of the afflicted artery) within six months after treatment. Since restenosis can lead to myocardial infarction (an area of necrosis in the heart muscle resulting from obstructed local circulation) and death and is estimated to cost over $2 billion annually to treat,[1] clinicians hope that improvements in diagnostic techniques and angioplasty assessment will reduce the failure rate by enabling the subtle aspects of restenosis-related vessel physiology to be understood.

Angioplasty results are assessed using only static arteriograms (roentgenographic images of arteries into which a contrast-enhancing radiopaque medium has been injected). In simplified terms, a successful angioplasty is declared when the treatment results in an arteriogram of an opened artery. Yet, evidence suggests that restenosis may be related to disturbances in the local flow at or near the blockage site. If these disturbances were observable during angioplasty, the procedure could be modified to lessen their effect. Of course, the flow state around a blockage site cannot be interpreted by looking at static images of an artery. Our objective, therefore, has been to demonstrate the feasibility of obtaining flow-disturbance information by processing a sequence of images obtained by conventional coronary arteriography without supplementary measurements or instrumentation. The initial demonstration used actual fluid flows in simple models of coronary arteries for conditions of steady flow observed with clinical arteriographic equipment. To confirm the experimental results, we computed a numerical simulation for flow conditions as close as possible to those of the laboratory study. Finally, to demonstrate the method for more realistic physiologic conditions, and as a point of reference for relating the steady-flow results to flows more characteristic of coronary flow, another numerical simulation was conducted for nonsteady pulsatile background flows.

The following are the major conclusions of our study:

1. Useful flow-related information is obtainable from processed arteriograms for the conditions considered.
2. A cost-effective and convenient means of obtaining flow information is available, given the frequency of coronary arteriography.
3. A possible path exists for obtaining the additional diagnostic information that may help reduce the incidence of life-threatening restenosis.

We have made several simplifying assumptions discussed later that will require further consideration before clinical application is possible.

The use of simulated blood flow and arterial models has led us to consider the broader implications and uses of these tools and is the reason we are contributors to this theme issue on synthetic environments. In the concluding remarks, we will discuss the possible applications of a synthetic artery that could evolve from this early simulation work and the benefits that would be derived.

THE RELEVANCE OF HEMODYNAMICS

Angioplasty, formally known as Percutaneous Transluminal Coronary Angioplasty (PTCA), involves the inflation of a balloon inside a severely narrowed artery to reopen the vessel and reestablish blood flow following deflation.[2] It is a relatively noninvasive treatment compared with the most common alternative: a bypass graft attached during open-heart surgery. Angioplasty

was introduced in 1977, and more than 300,000 PTCA procedures are now performed annually.

The primary means for assessing the condition of an artery before and after angioplasty is arteriography. Arteriography is the video or film capture of the X-ray shadows cast by a contrast-enhancing radiopaque medium injected into an artery. An example of an arteriogram from a patient study of a bypass graft is shown in Figure 1. A radiopaque agent is necessary, since the X-ray absorption characteristics of blood, vessels, and surrounding tissue are similar, and image contrast would thus otherwise be insufficient to define the edges of a vessel clearly enough for an accurate diagnosis. Because arteries are attached to the heart, which is moving, multiple images are acquired at high speed during arteriography to ensure that at least a few of them will be at the desired orientation and to obtain the proper position of the injected contrast material as it is carried through the vessel. Several new diagnostic techniques are in development using magnetic resonance imaging (MRI) and ultrasound imaging, but arteriography is the method of choice for assessing coronary artery disease and is almost exclusively used in grading the success of PTCA.

The first step in PTCA is the catheterization of the patient, which entails placing a small tube carrying the contrast medium, a balloon, and air to inflate the balloon, into an artery. Injections of radiopaque material are made, and images of the artery are obtained before and after angioplasty. Once the obstruction appears to be relieved (i.e., the amount of the contrast agent in the previously blocked portion of the artery roughly equals that in nearby unblocked segments), the catheter is withdrawn.

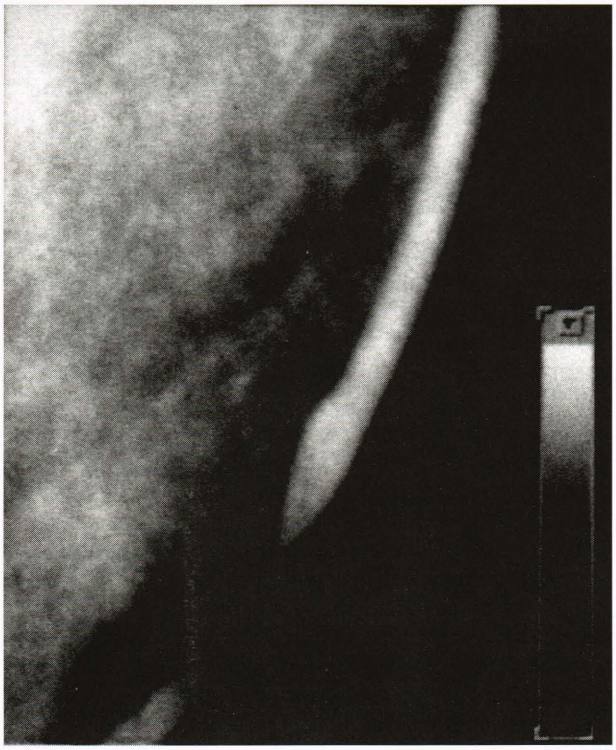

Figure 1. An arteriogram of a severely (> 90%) stenosed bypass graft. Note that the contrast agent is nearly unobservable in the narrow portion of the vessel in the lower left corner of the arteriogram.

Unfortunately, arteries opened in this way tend to close spontaneously shortly after treatment. The restenosis rate six months after initially successful angioplasty, referred to as late restenosis, is estimated to be 30%.[1] The reasons for this phenomenon are not fully understood, but effects related to the dynamics of blood flow, a field of study called hemodynamics,[3,4] and their interaction with structural properties of the lesion[5] appear to be contributive. Characterizing the flow environment near a treated lesion, even approximately, may be useful in predicting the likelihood of restenosis.

Cardiologists performing arteriography have reported observing apparent variations in the streaming of the contrast agent into an artery during injection, but such observations were tentative at best. We sought to process a sequence of arteriograms in a way that would enhance whatever flow-sensitive information was contained in the images. More direct means of accessing blood-flow characteristics are available using additional instruments such as a Doppler ultrasound velocimeter, which is a catheter-based device for direct measurement of flow velocity. Mean background flow can also be measured using phase-contrast MRI.[6] Our approach, however, because it involves extracting supplemental information from commonly obtained arteriograms with little additional clinical effort and no significant extra cost or inconvenience to patient or physician, is more likely to be used routinely. The total development time and additional expenses, moreover, are expected to be less than for more elaborate techniques.

The approach we developed[7,8] is intended to signal the presence of flow disturbances in an artery but does not offer accurate hemodynamic information owing to limitations inherent to arteriography. Since the image formed under arteriography is a two-dimensional projection of a three-dimensional object, and since the radiopaque medium is miscible with blood, a complete description of the flow is not possible, but an indicator for the presence and extent of a flow disturbance was hypothesized.

To demonstrate our method, we conducted a series of laboratory experiments in collaboration with cardiologists from the Johns Hopkins School of Medicine involving steady flows in acrylic models to obtain a set of arteriograms under controlled conditions. Flows from steady rather than pulsatile background pressure were studied because they are easier to produce and control and provide a good first approximation to the overall dynamics of pulsatile flows.[9,10] The approximation is acceptable at physiological pulse and flow rates for human coronary arteries of 4-mm diameter or less.[11] Although the diameters of the model arteries used in this study are larger, the dynamics are equivalent to flows in smaller vessels because, according to the principle of dynamic similarity,[12] dynamics are equivalent as long as the proper ratio of dimensions, velocity, and forces is maintained. This principle makes it possible to conduct aerodynamic studies using small-scale aircraft in wind tunnels. Thus, a convenient size of the arterial model was constructed that best matched the physical conditions of the pumps, tubes, and accessories available for the experiment.

A measure of dynamic similarity is the Reynolds number, which will later be described and related to these experiments. Results obtained in applying the method to the *in vitro* contrast flows were compared with those from numerical simulations of the experimental flows. The numerical simulations were successful in confirming the results obtained from the laboratory flows. Additional numerical studies of the method for nonsteady background pressures[8] were conducted to demonstrate the behavior of the method for more realistic pulsatile background flows.

MATERIALS AND METHODS

Parametric Image Calculation

Parametric arrival time and turbulence images of flow-sensitive parameters were computed from a sequence of arteriograms to describe the flow state in an artery. A parametric image contains pixels whose color or intensity describes some aspect of the object at that pixel location. Parametric imaging can be thought of as a filtering operation. The input is the array of time-varying pixel intensities, and the output is one or more images of the desired parameter values calculated from the underlying input pixels. The technique has been used in a variety of cardiac imaging applications.[13]

In our study, parametric images were calculated from the contrast density curve at each pixel in an arteriogram obtained for the entire passage of the radiopaque bolus. The pixel locations were determined by the arteriograms. The contrast density curve is simply a plot of pixel intensity as a function of time corrected for background variations and is typically Gaussian, but with varying spread, for a complete passage of the contrast material. An idealized contrast density curve for an arriving bolus is shown in Figure 2. A similar mirror image curve would represent a departing bolus. The duration of the maximum is a function of the amount of contrast agent injected. Since arteriographic images from a patient examination are mathematically processed via coordinate transforms to ensure proper registration, a given pixel corresponds to the same anatomical location, frame to frame, despite motion due to respiration, the pulsation of the heart, and inadvertent camera movement. Each region of interest in an arteriogram is linearly warped, a mathematical method of aligning dissimilar images,[14] to coincide with the same region of interest in every other arteriogram of a sequence. In laboratory studies involving stationary tubes, a far simpler case than that for moving arteries, small inadvertent movements due to camera tremor or other sources are corrected simply by translating and rotating each image in a sequence to match the position of the first image. By observing variations in the rate and appearance of contrast-agent filling at a particular pixel, it has been possible to perceive flow effects not readily detectable otherwise.[15,16]

A flow-sensitive parameter indicative of the contrast medium's arrival time was calculated using the times t_1 and t_2 obtained from the contrast density curve, as shown in Figure 2. The curve was formed as the frames were acquired, and t_1 and t_2 were derived from postprocessing

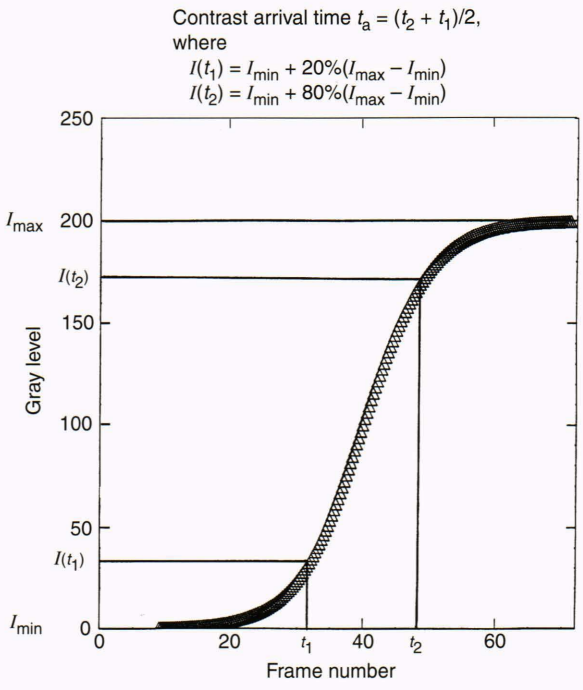

Figure 2. Idealized contrast density curve for an arriving radiopaque bolus. The time t_1 is the instant (frame number) the intensity I corresponding to contrast density has achieved 20% of its total increase from baseline to its maximum value, and t_2 is the time it has achieved 80%. The pixel values in the arrival time parametric image equal $(t_2 + t_1)/2$, which approximately represents the midpoint in the curve.

the curve. The times obtained from the curve actually represent frame numbers. The frames used in this study, as in most arteriographic applications, were acquired at 1/30-s intervals. The first-acquired frame was assigned a time of zero, and all subsequent frames were counted from it. The time t_1 is the instant (frame number) the contrast density has achieved 20% of its total increase from baseline to its maximum value, and t_2 is the time it has achieved 80%. The pixel values in the arrival time parametric image equal $(t_2 + t_1)/2$, which approximately represents the midpoint in the curve. This point was computed, since it is sensitive to movement of the contrast material but is likely to be less susceptible to measurement error than attempting to estimate the actual maximum value of the curve precisely. The resultant image was then intensity stretched to facilitate interpretation, which is a process that emphasizes the difference between minimum and maximum pixel values to make variations more easily detectable by observation.

We also defined a turbulence parameter and generated corresponding turbulence parametric images that were calculated from variations in the intensity of the high-frequency components of the Fourier transform of the contrast density curve. The turbulence image index was calculated from the fast Fourier transform (FFT) of the same contrast density curves used for the arrival time images. Since the equations given below, which were used to compute the turbulence parameter, sum a portion of the high-frequency components of the FFT as a relative

measure of the high-frequency contribution in a particular contrast curve, curves containing significant high-frequency activity, assumed to be correlated to turbulent flow, can be distinguished from those that do not. A sum of components was chosen as the turbulence measure to provide a more robust index of turbulent activity than a single component value. The general form of the turbulence index for a pixel at row i and column j of an N point (i.e., formed from measurements on N frames) contrast density curve is

$$x_{i,j} = \frac{1}{R} \sum_{q=k}^{m} a_{i,j}(q), \quad (1)$$

where R is a normalizing factor defined in Equation 2, m is the arbitrarily defined upper limit of the turbulence component range, k is the lower limit, and $a_{i,j}(q)$ is the qth frequency component of the FFT's magnitude defined in Equation 3. Pixel values in the parametric images of this index were obtained for a low-frequency range ($k = 1$, $m = 38$) and a high-frequency range ($k = 39$, $m = 58$), identically scaled, and then compared. The ranges selected for m and k were empirically established. The normalizing factor is defined as

$$R = \sum_{q=1}^{NF-1} a_{i,j}(q), \quad (2)$$

where NF is the number of components in the FFT, and $a_{i,j}(q)$ is the qth frequency component of the magnitude of the FFT as defined by

$$a_{i,j}(q) = \{\mathrm{FFT}^{*}(cd_{i,j}(t)) \times \mathrm{FFT}(cd_{i,j}(t))\}^{1/2}(q), \quad (3)$$

where $cd_{i,j}(t)$ is the value of the contrast density curve at row i, column j, and time t, and $0 < t < (N-1)\Delta t$. For the 30-frames/s acquisition rate used in obtaining the arteriograms, $\Delta t = 33$ ms, and the maximum value of q is 15 Hz, the Nyquist frequency. Fast Fourier transforms of 128 points were calculated ($NF = 128$).

Computational Facilities

A Silicon Graphics RS4000 Entry Indigo has been used as the computational platform for the project. A versatile software package, the Fluid Dynamics Analysis Package (FIDAP), from Fluid Dynamics International, Inc., is installed on the Indigo and is used to carry out the simulation of fluid dynamics. The FIDAP software is a finite element method analysis package consisting of three modules: (1) a mesh generation module that automatically divides the flow domain into discrete, contiguous elements, (2) a solution module that solves the governing equations, and (3) a postprocessor for graphical representation of the field variables. The Indigo is configured with an S-Video board that permits real-time capture of screen text and graphics on VHS videotape for archival and didactic purposes. Also installed on the Indigo is the Interactive Data Language (IDL) software package from Research Systems, Inc., which is employed for user interface development, animation, warping, contrast enhancement, and other image processing functions.

Laboratory Studies

Arteriogram sequences were acquired under steady background conditions for constricted and unconstricted acrylic models of an artery (see Fig. 3) designed for this experiment, and flow-sensitive parametric images were derived. The models consist of two 75-in.-long, 0.5-in.-dia. inlet and outlet sections connecting to a variable output pump and drain and a set of interchangeable 2-in. central sections of 0.5-, 0.4-, 0.25-, 0.15-, 0.05-in. diameter (0%, 20%, 50%, 70%, and 90% reduction). Two

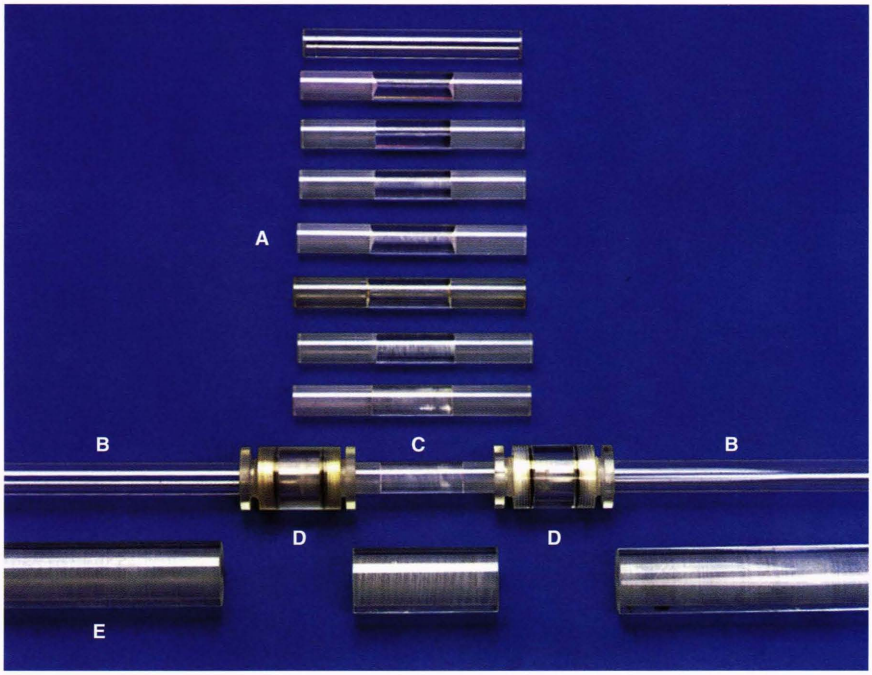

Figure 3. Acrylic model of an artery. **A.** Central test sections with various constrictions. **B.** Inflow-outflow sections. **C.** Test section attached to inflow-outflow connectors. **D.** Connectors. **E.** Attenuation-scatter equalizing sleeve.

versions for each diameter are available: one with a 90° exit-entrance angle and another with a 135° exit-entrance angle. Thus, ten interchangeable central test sections are in use, and more can easily be added if necessary. The test sections are connected to the inlet-outlet tubes by watertight acrylic connectors. Sleeves are placed over the inlet, outlet, and test sections of the same dimensions as the connectors to provide uniform X-ray scatter and attenuation across the entire model. Only the 0% (unconstricted) and 50% diameter-reduced (75% area constriction) test sections were used for the experiments reported here.

The nominal flow (from left to right) in the models for all tests was 8.3 ± 0.1 ml/s, using water as the working fluid, which corresponds to a Reynolds number of 821, a value representative of coronary arteries.[11] The flow rate was measured at the drain site using a graduated cylinder and stopwatch. A 20-ml bolus of sodium iodide in water (40 g NaI/100 ml) was introduced through a side arm at the start of the inflow section. The 35-mm cine images were acquired just downstream of the stenosis section using a GE Fluoricom 5000 X-ray system at a constant source-intensity setting, 6-in. magnification, and 30-frames/s acquisition rate.

The developed film was mounted on a standard viewing projector for 35-mm film with a beamsplitter directing images onto the aperture of a charge-coupled device camera for digitization. The images were digitized to form 384 × 512 image arrays and stored. The parametric images were calculated using the contrast density curves, as described earlier.

Numerical Simulation

The numerical simulation was carried out by solving Navier-Stokes equations for continuity and momentum for the axial and radial dimensions. The equation for continuity is

$$\nabla \cdot \mathbf{v} = 0 , \tag{4}$$

and the radial (r) momentum is determined by

$$\frac{dv_r}{dt} = -\frac{\partial p}{\partial r} + \frac{1}{Re}\nabla^2 v_r - \frac{1}{r}\frac{\partial}{\partial r} < r v_r'^2 > - \frac{\partial}{\partial z} < v_r' v_z' > , \tag{5}$$

where $\mathbf{v}$ is the velocity vector, v_r is the radial velocity component, v_z is the axial velocity component, p is pressure, v_r' and v_z' are fluctuating components of velocity, and $< >$ represents the correlation. A similar equation exists for the axial (z) momentum. The Reynolds number Re is defined as $\rho u l/\mu$, where ρ is the fluid density, u is the reference velocity, l is the reference length, and μ is the fluid viscosity. The continuity equation, which states that mass is conserved, must be satisfied throughout the flow domain. The radial momentum equation expresses the balance of forces in the radial direction. Equation 5 relates the total derivative of velocity to the pressure gradient, viscous diffusion, and the turbulent stresses (last two terms).

A two-dimensional geometrical model of the acrylic tube designed for the laboratory experiment was computer coded and used to produce a numerical simulation of the flow field in the tube. A two-dimensional model was chosen, since the flow in an axially symmetric straight tube is assumed to be two-dimensional axisymmetric. The finite element method[17] was used to solve for the flow in the geometrically defined model. In this technique, a region of space in a specified geometry, here the modeled vessel, is divided into small, contiguous elements much like the process of covering a floor with rectangular tiles. The "tiles" that define the computational domain for the arterial model are shown in Figure 4. The Navier-Stokes equations, which are used to characterize flow, were numerically solved within this computational domain. Dividing the model into small elements enables complex flows to be computed by solving for linear variations of the dynamical variables across an element and linking these results by matching boundary values. Solution of complex flows in an extended object would otherwise be prohibitively difficult to model. It is important, however, that the elements be sufficiently small to allow a linear approximation to the equations of flow within that region to prevent errors from being introduced. Care was therefore taken to use a finer grid near the wall boundaries (see Fig. 4) and in the vicinity of expected recirculation zones to resolve the high gradients known to exist in those regions better.[9,18]

Turbulence in the governing equations was accounted for through the two-equation turbulence model, which requires solution of two extra equations, one for the turbulence intensity k and one for the turbulence dissipation rate ϵ. The k (the autocorrelation $<u'u'>$, where prime denotes the fluctuating quantity of the reference velocity u and $< >$ implies time correlation) is used to characterize turbulent energy and serves as a comparative quantity for parametric turbulence images derived experimentally from arteriograms. The nominal grid was a 3276-element quadrilateral with each element having four nodes. Converged solutions were achieved through the Galerkin method,[19] and mass conservation was satisfied by the penalty approach (i.e., the same mass leaves as enters a grid element). Solutions for 0% and 75% area constricted models were obtained, and the geometry and Reynolds numbers were matched to the experiments. The boundary

Figure 4. Finite element grid near a constriction.

conditions for the inlet velocity profile were specified as laminar parabolic.[20]

To simulate the flow of the contrast agent, we introduced a series of massless tracer particles proximal to the constriction and tracked their path as they traversed the model. Since massless particles were used, the flow was not affected by their presence. Because the numerical simulation utilized particles to track the location of the contrast medium, the arrival of a particle at a particular location was associated with finding the midpoint of the contrast density curve. The numerical simulation arrival time parameter was therefore the time a massless particle, introduced at the inlet plane, reached a given location.

Results

The parametric images generated in the studies are summarized in Table 1.

Table 1. Summary of parametric images and experimental conditions used to generate them.

Area constriction	Laboratory/ simulation	Parametric image	Figure
75%	Laboratory	Arrival time	5A
0% (control)	Laboratory	Arrival time	5B
75%	Laboratory	Turbulence	6A
0% (control)	Laboratory	Turbulence	6B
75%	Numerical simulation	Arrival time	7A
0% (control)	Numerical simulation	Arrival time	7B
75%	Numerical simulation	Turbulence	8

Steady Flow

We calculated parameters from the laboratory-acquired arteriograms using the method described earlier. Arrival time images of the radiopaque bolus (Figs. 5A and 5B) and turbulence images (Figs. 6A and 6B) were calculated for arteriogram sequences of both the 75% area constricted and unconstricted models. (Note that the arteriograms of the experimental flows were acquired at an angle of about 45° relative to the edge of the film. All flows were horizontal, however.) In the figures, the pixel brightness intensifies with increasing arrival time and turbulence. Bright areas next to the exit of the constricted portion of the model in Figure 5A suggest delayed filling caused by recirculation known to exist at this Reynolds number for a stenosis of this severity.[18] No such regions are present in the straight tubes, where the flow does not recirculate at this Reynolds number (Fig. 5B).

The arrival time parametric images obtained from the numerical simulation for a central cross section of the model are shown in Figures 7A and 7B. X-ray attenuation and three-dimensional geometry effects have not been included in the arrival time computation. Pixel intensity becomes more pronounced as the arrival time for a particle increases. The simulation-derived turbulence image for the 75% area constricted model is shown in Figure 8. The pixel intensity increases as turbulence intensifies, as described earlier. The turbulence image for the unconstricted model is virtually uniform and is not shown. Streamlines (Fig. 9) and shear forces (Fig. 10) computed by the numerical simulation are also shown.

Numerical Simulation: Pulsatile Background Pressure

To study the performance of parametric imaging for more physiologically realistic background flows, we conducted a pulsatile flow simulation using the same model geometry and governing equations. The waveform for the inlet pressure is shown in Figure 11. The peak Reynolds number for the flow was 821, matching that used in the steady-flow studies. Again, a series of massless tracer particles were released, and their position throughout the model was recorded as a function of time. As with the steady-flow simulation, an arrival time image was obtained for a center cross section of the obstructed model (Fig. 12). The dark regions next to the model

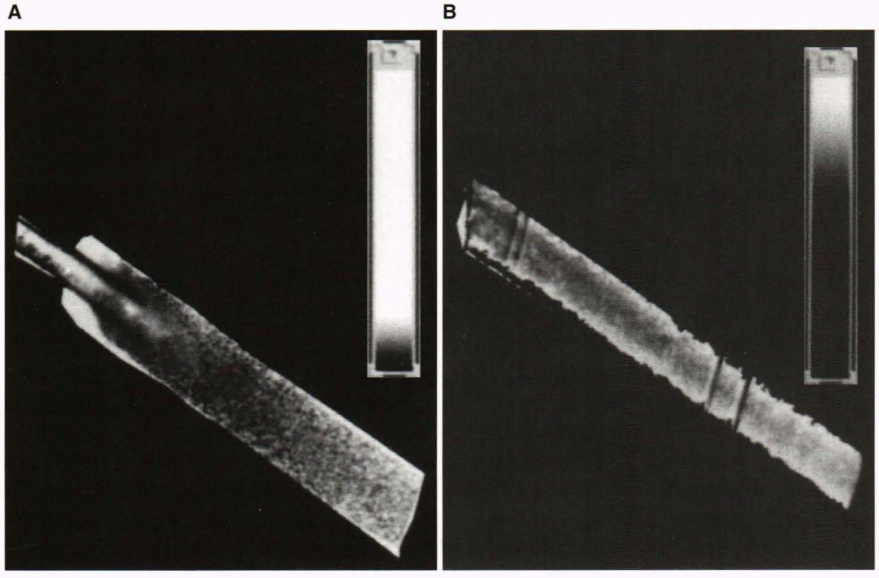

Figure 5. Arrival time images for the radiopaque bolus. (The flow is from left to right.) **A.** Laboratory model with 75% area constriction. **B.** Unconstricted model.

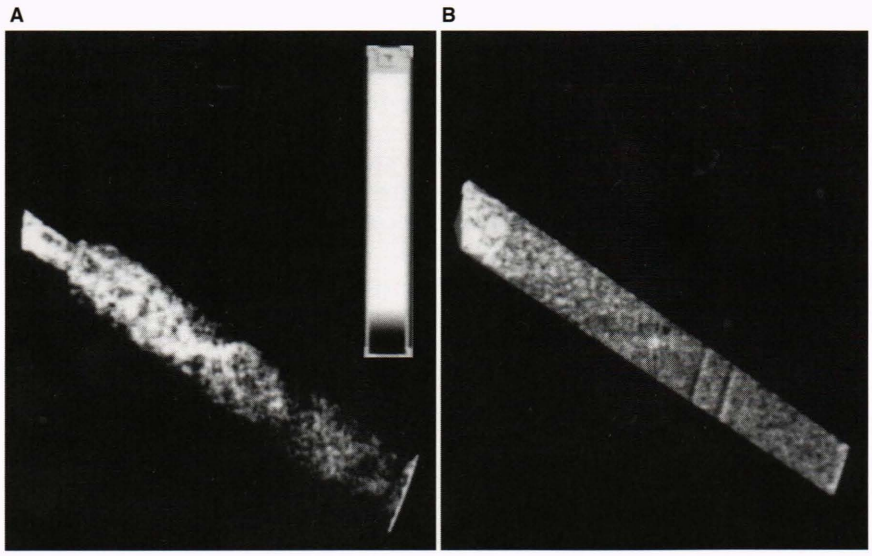

Figure 6. Turbulence images. (The flow is from left to right.) **A.** Laboratory model with 75% area constriction. **B.** Unconstricted model.

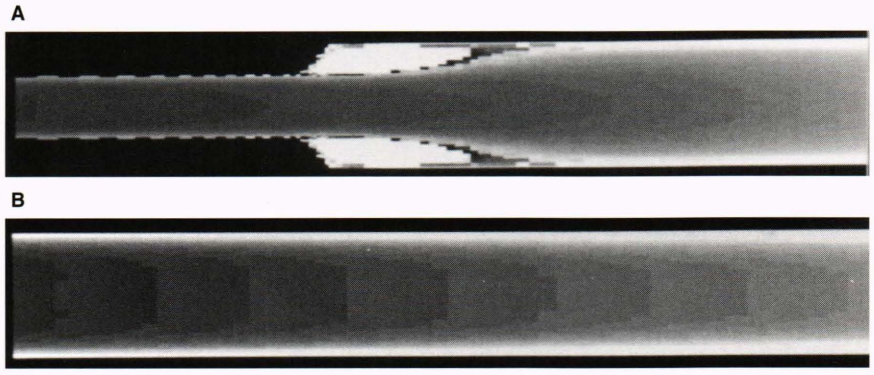

Figure 7. Numerical simulations of the arrival time for the radiopaque bolus in a central cross section of the model. (The flow is from left to right.) **A.** Simulation for 75% area constriction. **B.** Simulation for 0% constriction.

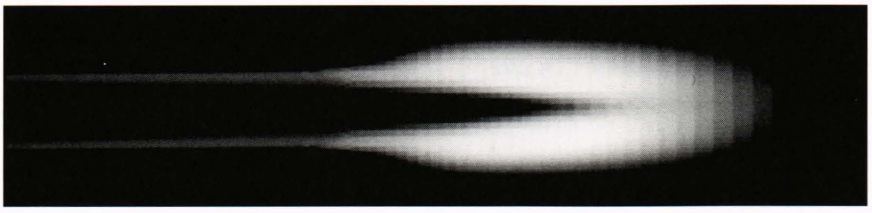

Figure 8. Turbulence simulation for 75% area constriction. (The flow is from left to right.)

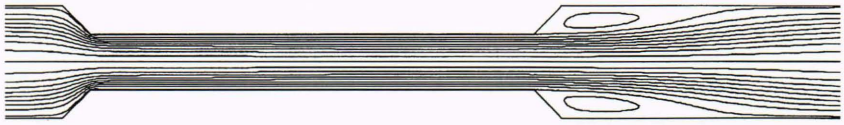

Figure 9. Simulated streamlines for the steady-background flow in the presence of a 75% area constriction.

artery's wall below (distal to) the constriction that received no contrast material during the simulation are completely black. Streamlines for the pulsatile simulation at selected times are also shown (see Fig. 13).

Cinearteriographic Simulation

In obtaining parametric images from the numerical modeling, we also demonstrated a new capability for simulating cinearteriographic contrast injections, first for steady flows (see inside back cover) and later for pulsatile flows.[8] Sixteen frames of a fifty-frame animation of the pulsatile study are shown in Figure 14. The frame numbers correspond to the frame number in the animation (e.g., frame 25 is the 25th frame in the animation). The fifty frames span one cycle of the input background pressure pulse. Note how the contrast agent breaks up and accumulates in the recirculation zone and along the walls of the model. For the simulation, only a small amount of

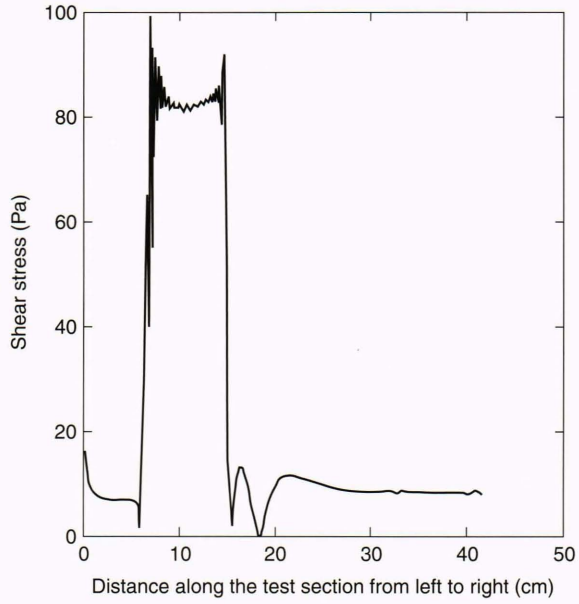

Figure 10. Shear stress computed from simulated flow along the wall of the model artery with a 75% area constriction.

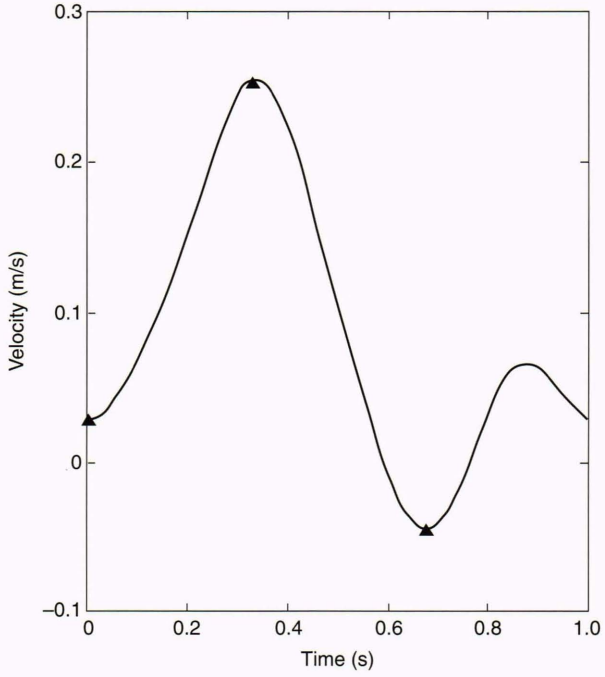

Figure 11. Inlet axial velocity waveform. The triangles denote the times (t = 0, 0.325, 0.675 s) during a pulse at which the streamlines in Figure 13 were plotted. The pulse duration is 1 s. (Adapted, with permission, from Ref. 21, p. 1148. © 1992 by Elsevier Science Ltd., The Boulevard, Langford Lane, Kidlington, U.K.)

contrast material was injected. In actual practice, quantities sufficient to fill the vessel completely for a brief period are supplied. The animation depicts the release of several massless tracer particles in the flow for a two-dimensional slice through the center of the vessel, as described earlier. The X-ray illumination along a given line of sight for a set of parallel ray directions is blocked if a particle is encountered; otherwise, it passes unattenuated. The animation shows the radiopaque bolus wavefront as it travels through the vessel, revealing various details of the flow, including the size variation of the recirculation zone during the cardiac cycle. This animation capability has been helpful in considering new simulation applications, as discussed in the section on future work.

DISCUSSION

Steady Flows

The parametric images derived from the model flow experiments are very similar to the numerically simulated result. Recirculation zones on either side of the constriction at its exit and areas of jetting along the tube walls of the constricted portion of the vessel are clearly visible in both cases in about the same locations. The sizes of the recirculation and turbulence zones are consistent with published, precise measurements made from a range of Reynolds numbers that spanned the value of 821 used here for a similar model of a stenosed artery.[11] The streamline calculations obtained with the simulation (Fig. 9) also demonstrate recirculation zones in this region. Thus, the goal of proving the possibility of identifying regions of disturbed flow was met for the conditions studied.

A jetting phenomenon is observable in the arrival time images (Figs. 5A and 7A) at the exit of each constriction and was examined in detail using the velocity distribution calculated by the finite element simulation. The jetting was discovered to be the result of the increased flow velocity at the inlet of the constriction generated as fluid near the wall in the unobstructed portion of the model is forced into the narrowed section of the tube. The high-velocity region persists through the contracted area until the fluid velocity decreases below the obstruction, creating a jetlike structure.

The distinct region of high-frequency variation shown in the turbulence image of Figure 6A in comparison with that of Figure 6B suggests that a turbulent region is present, particularly since low-frequency parametric images (not shown) obtained with the constricted model demonstrate no such variation. The extent of the turbulence region observed in the numerical simulation

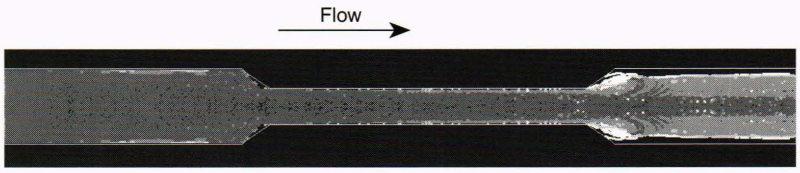

Figure 12. Simulated arrival time image for the radiopaque bolus in the presence of a 75% area constriction under the pulsatile-background flow conditions.

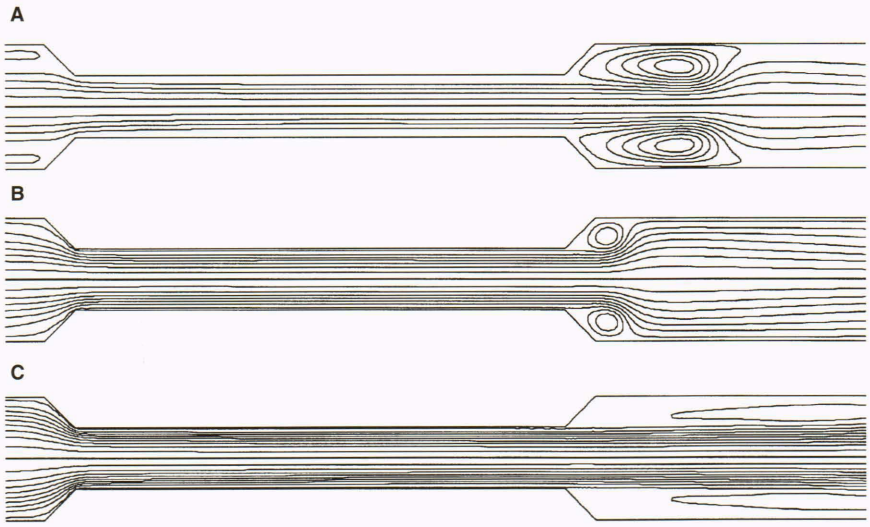

Figure 13. Streamlines during a pulse (refer to Fig. 11). **A.** 0 s. **B.** 0.325 s. **C.** 0.675 s.

(Fig. 8) is consistent with the parametric turbulence image.

The shear force distribution results (Fig. 10) agree qualitatively with earlier *in vitro* measurements[22] made in flow-through casts of human arteries. As in those studies, shear forces dramatically increase distally (downstream) from the reattachment point, a point of local shear minimum.

Pulsatile Simulation

The presence of a recirculation zone, as suggested in the steady-flow parametric image, is evident in the pulsatile result as well, although its appearance is more structured. Streamlines for the pulsatile flow are shown in Figure 13. They reveal the changing nature of the recirculation zone throughout a pulse cycle and help explain the complexity of the pulsatile arrival time image compared with that of the steady-background flow simulation.

Approximations

Several approximations were made to accomplish the demonstration and numerical flow modeling. The acrylic "artery" and its corresponding numerical model are smooth, rigid, and straight, unlike actual arteries, which are tortuous and flexible. An ideal (Newtonian) fluid (i.e., one that has constant viscosity) was used in the experiments and simulations because blood behaves like an ideal fluid for vessels of 0.5-mm diameter or larger,[23] and the coronary arteries of interest have diameters larger than 1 mm. Also, since a single-phase, uniform fluid was used, multiphase flow effects at the wavefront were neglected. We have assumed that disturbances introduced by the catheter during injection will not significantly alter the results.

The finite element computations themselves approximate changes within an element and degrade with increasing object boundary complexity. Only a two-dimensional axisymmetric flow was considered, for the tube and the background pressures were axisymmetric. The boundary conditions were not directly measured but estimated on the basis of mean flow, tube length, and background pressure. Yet, for the intended purposes of confirming the results of our laboratory experiment and estimating the influence of pulsatile background pressure, the approximations seem justified and acceptable. The waveform used to provide pulsatile background pressure was derived, as mentioned earlier, from experimental measurements[21] and is only an example of arterial pressure, since pulsatile waveforms vary with size and location of the artery. The waveform will also be affected by catheter placement, injection pressure, and the onset time of injection relative to the cardiac cycle.

CONCLUSION

Our results suggest that flow turbulence and separation zone information are available from single-plane contrast arteriography. The additional information provided by parametric flow imaging may be useful in addressing the problem of postangioplasty restenosis, which has been somewhat difficult for clinicians to resolve with existing arteriographic analysis. Parametric imaging of flow disturbances is particularly attractive because it requires little additional clinical resources or effort to accomplish when implemented for conventional, single-plane arteriography. Should greater accuracy be necessary, biplanar arteriography, which acquires two images at separated angles and would facilitate three-dimensional imaging of the flow, is available in many hospital catheterization laboratories. Biplanar imaging, however, would require modification and retesting of the approach.

Further study is planned to probe the limitations of the approach and to develop a more faithful test environment that takes vessel compliance and curvature into account and uses numerical simulation tools. Numerical simulation offers a powerful means of modeling arterial physiology, blood flow, and diagnostic techniques without the expense, logistical complications, intricate machining, and drenched clothing that often accompany laboratory experiments with fluids.

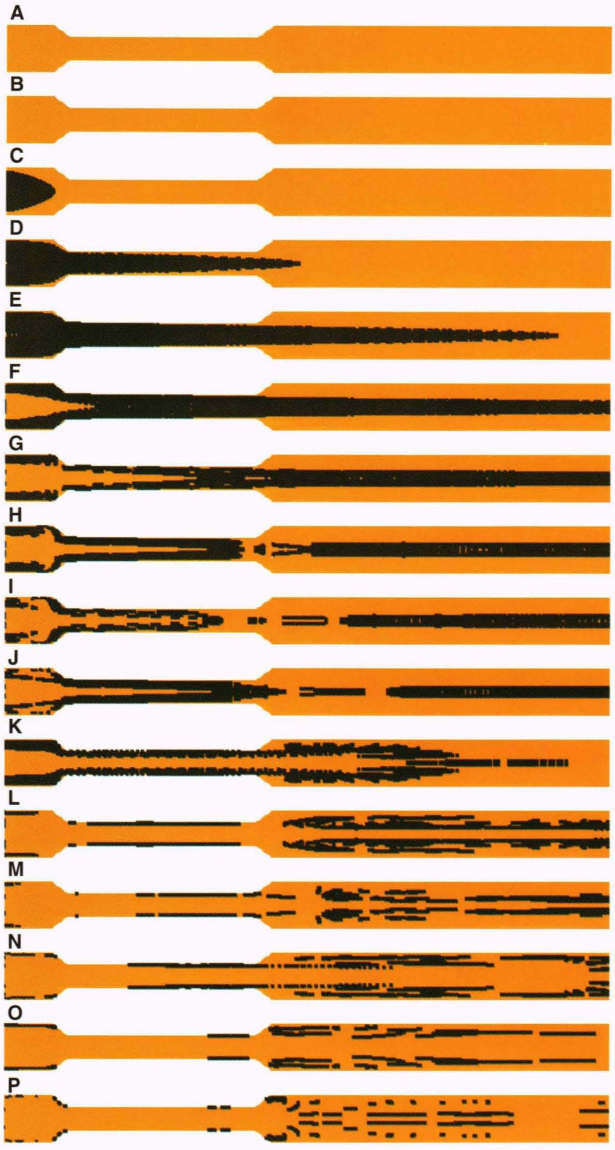

Figure 14. Sixteen frames from a fifty-frame animation made during the pulsatile-flow study of a simulated contrast medium injection. (The flow is from left to right.) **A.** through **J.** Frames 1 through 10. **K.** Frame 15. **L.** Frame 20. **M.** Frame 25. **N.** Frame 30. **O.** Frame 40. **P.** Frame 49. Frames 1 through 50 represent one cycle of the pulse (see Fig. 11).

FUTURE WORK

We hope to extend the blood-flow simulation to include the material properties of the vessel, also modeled using finite element method techniques, with the aim of developing a synthetic artery for use as a more general coronary research and assessment tool. The ability to simulate arterial hemodynamics faithfully would have benefits beyond the immediate application of arteriography. Inclusion of material properties models would permit the effects of compliance on hemodynamics to be considered. Conversely, the impact of hemodynamics on vessel structure could also be studied. Hemodynamic interactions with the mechanical properties of the wall are believed to play a major role in atherogenesis (long-term formation of lesions in the arterial wall), in restenosis following balloon angioplasty, and in the onset of symptoms, including myocardial infarction, in previously asymptomatic coronary artery disease patients. For example, plaque, a constituent of atherosclerotic lesions, may rupture as a result of material fatigue caused by hemodynamical forces,[24] which may in turn lead to flow-limiting clot formation. Yet many plaques develop only small fissures that heal without consequence and pose no threat to the patient. A method is needed for examining the mechanical properties of plaques and considering the influences of hemodynamics on the development of stress cracks in plaques.

The creation of a synthetic artery, although an undertaking requiring substantial resources to accomplish, will offer a unique ability to study and probe questions of coronary health not easily addressed otherwise. Another research opportunity using this capability is the design of a virtual catheterization environment for training and surgical planning. Development of this environment will require the incorporation of force-feedback devices to simulate catheter tension, balloon pressure, and three-dimensional imaging. A student using the tool could train and learn from an extensive set of catheterization exercises, thus offering educators greater control of the training environment and assuring a thorough exposure to the major issues in catheterization. The virtual catheterization environment would permit improved evaluation of students using standardized materials and unlimited opportunities for practice without exhausting the supply of test materials or fear of patient or animal injury. Such a simulation tool would also offer treatment advantages, since it could be used by the clinician to plan catheterization or angioplasty or to consult with other clinicians in a lifelike, interactive fashion. This pilot study is, of course, a small step along the path to a synthetic artery, but continued evolution of this and other simulation tools integrated with additional sensory devices poses exciting possibilities for future medical applications.

REFERENCES

1. Wittels, E. H., Hay, J. W., and Gotto, A. M., "Medical Costs of Coronary Artery Disease in the United States," *Am. J. Cardiol.* **65**, 432-440 (1990).
2. Giuliani, E., "Percutaneous Transluminal Coronary Angioplasty," *J. Am. Coll. Cardiol.* **6**, 992 (1985).
3. Kuntz, R. E., Gibson, C., and Nobuyoshi, M., "Generalized Model of Restenosis After Conventional Balloon Angioplasty, Stenting and Directional Arthrectomy," *J. Am. Coll. Cardiol.* **21**, 15-27 (1993).
4. Nicolini, F. A., and Pepine, C. J., "Biology of Restenosis and Therapeutic Approach," *Surg. Clin. North Am.* **72**, 919-929 (Aug 1992).
5. Yock, P. G., Fitzgerald, P. J., Linker, D. T., and Angelsen, B. A. J., "Intravascular Ultrasound Guidance for Catheter-Based Coronary Interventions," *J. Am. Coll. Cardiol.* **17**, 39b-45b (1991).
6. Cline, H. E., Lorensen, W. E., and Schroeder, W. J., "3D Phase Contrast MRI of Cerebral Blood Flow and Surface Anatomy," *J. Comp. Asst. Tomg.* **17**, 173-177 (1993).
7. Raul, R., Geckle, W. J., Aversano, T., and Walford, G. D., "Visualization and Numerical Modeling of Disturbed Flows Observed in Cineangiography," in *Computers in Cardiology 1992*, IEEE Computer Society Press, Los Alamitos, Calif., pp. 323–326 (1992).
8. Geckle, W. J., Raul, R., and Aversano, T., "Effects of Simulated Pulsatile Background Flow on Parametric Visualization in Cineangiography," in *Computers in Cardiology 1993*, IEEE Computer Society Press, Los Alamitos, Calif., pp. 369-372 (1993).
9. Young, D. F., and Tsai, F. Y., "Flow Characteristics in Models of Arterial Stenoses—II. Unsteady Flow," *J. Biomechanics* **6**, 547-559 (1973).
10. Mates, R. E., Gupta, R. L., Bell, A. C., and Klocke, F. J., "Fluid Dynamics of Coronary Artery Stenosis," *Circ. Res.* **42**, 152-162 (1978).

[11] Solzbach, U., Wollschläger, H., Zeiher, A., and Just, H., "Effect of Stenotic Geometry on Flow Behavior Across Stenotic Models," *Med. Biol. Eng. Comput.* **25**, 543-550 (1987).
[12] Sommerfeld, A., *Mechanics of Deformable Bodies*, Academic Press, London, p. 261 (1950).
[13] Collins, S. M., and Skorton, D. J., *Cardiac Imaging and Image Processing*, McGraw-Hill, N.Y., p. 269 (1986).
[14] Russ, J. C., *The Image Processing Handbook*, CRC Press, Boca Raton, Fla., p. 96 (1992).
[15] Cusma, J. T., Toggart, E. J., Folts, J. D., Peppler, W. W., Hangiandreou, N. J., et al., "Digital Subtractive Angiographic Imaging of Coronary Flow Reserve," *Circulation* **75**(2), 461-472 (1987).
[16] Smedby, O., Fuchs, L., and Tillmark, N., "Separated Flow Demonstrated by Digitized Cineangiography Compared with LDV," *Trans. ASME* **113**, 336-341 (Aug 1991).
[17] Norrie, D., and DeVries, G., *An Introduction to Finite Element Analysis*, Academic Press, N.Y. (1978).
[18] Young, D. F., and Tsai, F. Y., "Flow Characteristics in Models of Arterial Stenoses—I. Steady Flow," *J. Biomechanics* **6**, 395-410 (1973).
[19] Cuvelier, C., Segal, A., and Steenhoveen, A. A., *Finite Element Methods and Navier-Stokes Equations*, D. Reidel Pub. Co., Dordrecht, The Netherlands (1986).
[20] Kleinstreuer, C., Nazemi, M., and Archie, J. P., "Hemodynamics Analysis of a Stenosed Carotid Bifurcation and Its Plaque-Mitigating Design," *ASME J. Biomech. Eng.* **113**, 330-335 (1991).
[21] Tu, C., Deville, M., Dheur, L., and Vanderschuren, L., "Finite Element Simulation of Pulsatile Flow Through Arterial Stenosis," *J. Biomech.* **25**, 1141-1152 (1992).
[22] Friedman, M. H., Deters, O. J., Bargeron, C. B., Hutchins, G. M., and Mark, F. F., "Shear-dependent Thickening of the Human Arterial Intima," *Atheroscler.* **60**, 161-171 (1986).
[23] Milnor, W. R., *Hemodynamics*, 2nd edition, Williams & Wilkens, Baltimore, p. 16 (1989).
[24] Constaninides, P., "Plaque Hemorrhages, Their Genesis and Their Role in Supra-Plaque Thrombosis and Atherogenesis," in *Pathobiology of the Human Atherosclerotic Plaque*, Glagov, S., Newman, W. P., III, and Schaffer, S. A., (eds.), Springer-Verlag, N.Y., pp. 393-411 (1990).

ACKNOWLEDGMENTS: We gratefully acknowledge the collaboration of Gary D. Walford, M.D., of St. Joseph's Hospital, Syracuse, N.Y., formerly of the Division of Cardiology of the Johns Hopkins Medical Institutions. His participation was supported by The Johns Hopkins University's Frank T. McClure Fellowship in Cardiovascular Research. The acrylic models were machined by the APL Technical Services Department, and software coding assistance was provided by Oba McMillan, a summer student employee.

THE AUTHORS

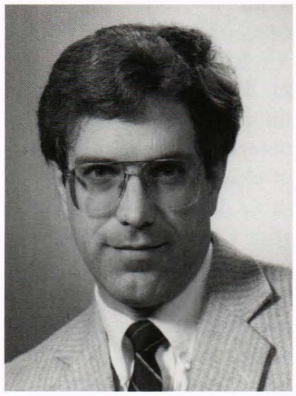

WILLIAM J. GECKLE is a Senior Staff physicist and software developer specializing in graphical interfaces and biomedical image processing in APL's Biomedical Research and Engineering Group. He received B.S. and M.S. degrees in physics from Loyola College in Baltimore, and Michigan State University, in 1977 and 1979, respectively. Mr. Geckle joined APL in 1979 as a member of the Associate Staff Training Program and later became a member of the Space Department, where he began working on collaborative biomedical projects. In 1984, he joined the Biomedical Programs Office, which was restructured in 1991 as the Biomedical Research and Engineering Group. Mr. Geckle is an instructor for the Armed Forces Institute of Pathology, Washington, D.C., in the telemedicine program and has recently completed a book chapter to be included in the second edition of *The Principles of Nuclear Medicine*.

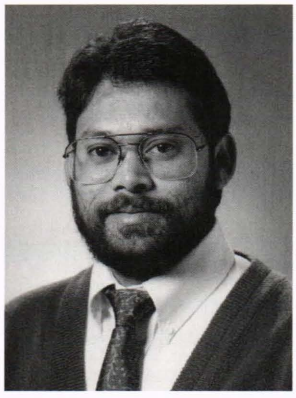

ROBIN RAUL received his B.S. in aerospace engineering from the Indian Institute of Technology, Kharagpur, in 1980, and his M.S. in aerospace engineering from the Indian Institute of Science, Bangalore, in 1982. He has also studied at the University of Maryland, where he received his Ph.D. in mechanical engineering in 1989. Dr. Raul joined APL's Milton S. Eisenhower Research Center as a postdoctoral research associate in 1989 and has been a member of the Senior Professional Staff since 1993. He has been conducting research in computational fluid dynamics, turbulence modeling, and biofluid mechanics.